

# Journal of Geophysical Research: Solid Earth

## RESEARCH ARTICLE

10.1002/2015JB012491

**Key Points:**

- Interplate locking in Lower Cook Inlet, AK, has varied over time between 1992 and 2014
- A slow slip event lasting at least 9 years long occurred from 1995 to 2004
- Slip on some sections of the megathrust may occur mostly or entirely through slow slip

**Supporting Information:**

- Supporting Information S1

**Correspondence to:**

S. Li,  
sli11@alaska.edu

**Citation:**

Li, S., J. Freymueller, and R. McCaffrey (2016), Slow slip events and time-dependent variations in locking beneath Lower Cook Inlet of the Alaska-Aleutian subduction zone, *J. Geophys. Res. Solid Earth*, 121, doi:10.1002/2015JB012491.

Received 2 SEP 2015

Accepted 30 DEC 2015

Accepted article online 5 JAN 2016

## Slow slip events and time-dependent variations in locking beneath Lower Cook Inlet of the Alaska-Aleutian subduction zone

**Shanshan Li<sup>1</sup>, Jeffrey Freymueller<sup>1</sup>, and Robert McCaffrey<sup>2</sup>**

<sup>1</sup>Geophysical Institute, University of Alaska Fairbanks, Fairbanks, Alaska, USA, <sup>2</sup>Department of Geology, Portland State University, Portland, Oregon, USA

**Abstract** We identify a series of abrupt changes in GPS site velocities in Lower Cook Inlet, Alaska, in late 2004, early 2010, and late 2011. The site motions during each time period are nearly linear. The surface deformations inferred from GPS for pre-2004 and 2010–2011 are similar to each other, as are 2004–2010 and post-2011. We estimate the slip distribution on the Alaska-Aleutian subduction plate interface accounting for upper plate block rotations and interpret this toggling between two deformation patterns as caused by transient slip. We find that by allowing negative slip deficit rates (i.e., creep rates in excess of relative plate motion), the data in Lower Cook Inlet are fit significantly better during pre-2004 and 2010–2011, suggesting the occurrence of slow slip events (SSEs) there during those time periods. The earlier SSE lasted at least 9 years (observations in that area began in 1995) with  $M_w \sim 7.8$ . The latter SSE had almost the same area as the earlier one and a duration of ~2 years with  $M_w \sim 7.2$ . During 2004–2010 and post-2011, the inversions result in only positive slip deficit rates (i.e., locking) in Lower Cook Inlet. Slip rates are nearly constant during the Lower Cook Inlet SSEs, and the events start and stop abruptly. Both of these properties contrast with observations of SSEs in Upper Cook Inlet and elsewhere. The Lower Cook Inlet SSEs are consistent with previously proposed duration-magnitude scaling laws and demonstrate that slow slip events can last as long as a decade.

## 1. Introduction and Background

### 1.1. Objective

Slow slip events (SSEs) are episodes of slip on a fault that are slow compared to the slip rates of normal earthquakes but fast compared to long-term fault slip rates. The basic description of an SSE is that a previously locked section of the fault slips for a while at a rate faster than plate motion then locks up again at the end of the event [Dragert *et al.*, 2001]. Unlike continuous steady creep, slow slip events (SSEs) occur with a finite duration and can involve fault slip rates that are faster than long-term relative plate motion. Considerable variability has been observed in the duration, magnitude, slip amount, and slip rate of SSEs [Schwartz and Rokosky, 2007]. Studies of SSEs provide significant insights into the dynamic mechanisms and physical conditions on the subduction plate interface [Peng and Gomberg, 2010].

Interseismic crustal deformation caused by the interplate locking on a subduction megathrust can be described using the basic model proposed by Savage [1983]. It is modeled as the sum of steady reverse slip representing the plate convergence and normal slip (back slip) to represent the slip deficit distribution on the plate interface. The interseismic velocity field can provide detailed information about the distribution of the slip deficit on the plate interface. The slip deficit over some time interval is defined as the expected slip on the plate interface (from plate motions) minus the actual slip. There are four different states of interplate locking on the plate interface [Ochi and Kato, 2013]: fully locked, partially locked, fully slipping, and overslipping. Fully locked indicates that there is no slip on the boundary so the slip deficit rate equals the plate convergence rate. Fully slipping means that there is no slip deficit, as the slip rate on the interface is equal to the plate convergence rate. Partially locked indicates that the locking rate is lower than plate convergence rate. Finally, the state of overslip would occur if the slip rate on the fault is faster than the plate convergence rate and may indicate the occurrence of the slow slip events [Ochi and Kato, 2013]. Here we examine the state of slip on a part of the Alaska megathrust and how it changes through time.

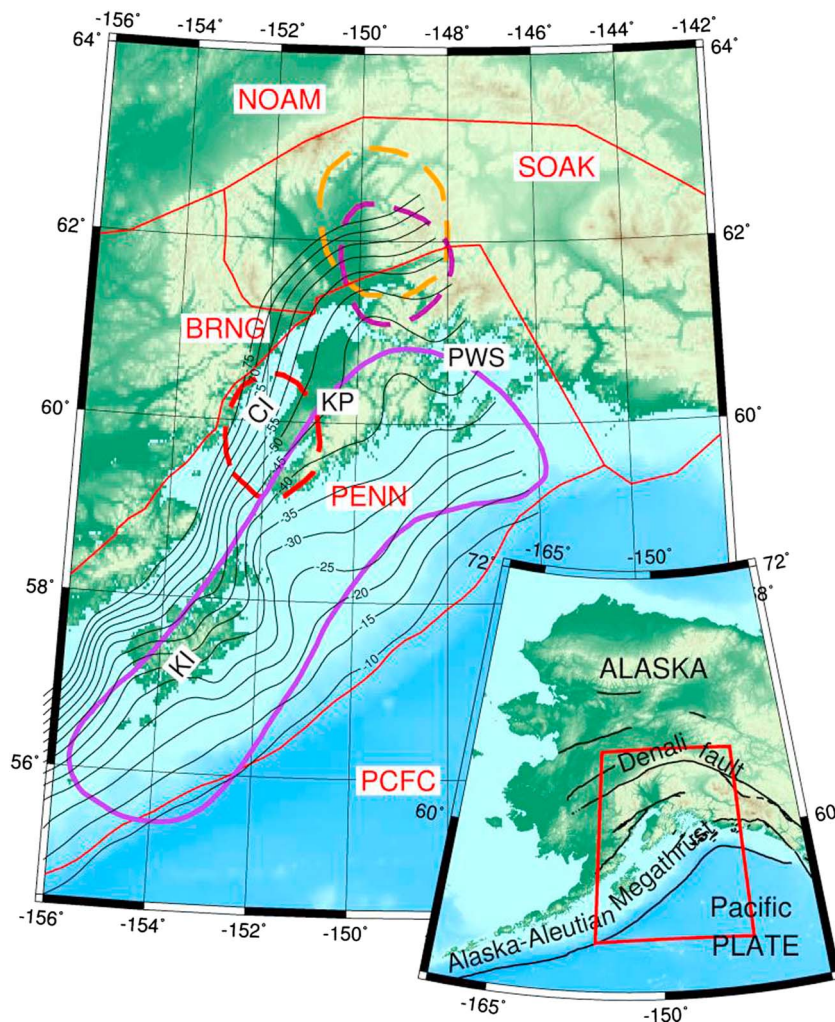


**Figure 1.** Topographic map and tectonic setting (inset) and study area in south central Alaska (red outline in inset map). Black solid lines are plate interface depth contours (in km) from Slab 1.0 [Hayes et al., 2012]. Red solid lines show the boundaries of blocks (named in red). Purple outline shows the approximate rupture extent of the 1964 earthquake from Furumoto [1965]. Purple dashed outline shows the 1998–2001 slow slip event [Ohta et al., 2006]; orange dashed outline shows the 2009–2013 slow slip event [Fu and Freymueller, 2013]; and red dashed outline shows the 2010–2011 slow slip event [Wei et al., 2012]. NOAM: North American Plate; SOAK: southern Alaska block; BRNG: Bering plate; PENN: Peninsula block; PCFC: Pacific Plate; Cl: Cook Inlet; KP: Kenai Peninsula; PWS: Prince William Sound; and KI: Kodiak Island.

### 1.2. Tectonic Setting

South central Alaska is a tectonically active region that features subduction, great earthquakes, and active volcanoes. The Alaska-Aleutian subduction zone, where the Pacific Plate subducts beneath the North American Plate (Figure 1), has the shallowest dip, close to  $3^{\circ}$  below the Kenai Peninsula, of any subduction zone in the world [Ohta et al., 2006]. At the eastern end of the subduction zone, a triangular-shaped block called the Yakutat terrane is colliding with Alaska, producing a collisional boundary between the subduction at the Aleutian megathrust and the Queen Charlotte-Fairweather transform fault [Elliott et al., 2013]. The exceptionally shallow dip of the subduction zone is related to this transition from simple subduction to collision. The convergence rate of the Pacific Plate relative to North America increases from  $\sim 55$  mm/yr near south central Alaska to 60 mm/yr along the Alaska Peninsula; in south central Alaska the convergence vector is rotated  $\sim 17^{\circ}$  clockwise relative to the trench-normal direction, while subduction is trench normal along the Alaska Peninsula. The upper plate in Alaska is characterized by major active faults like the Denali Fault (Figure 1), and all of southern Alaska moves relative to the stable North American Plate [Freymueller et al., 2008]. Several great earthquakes and long-term slow slip events have happened along the Alaska-Aleutian

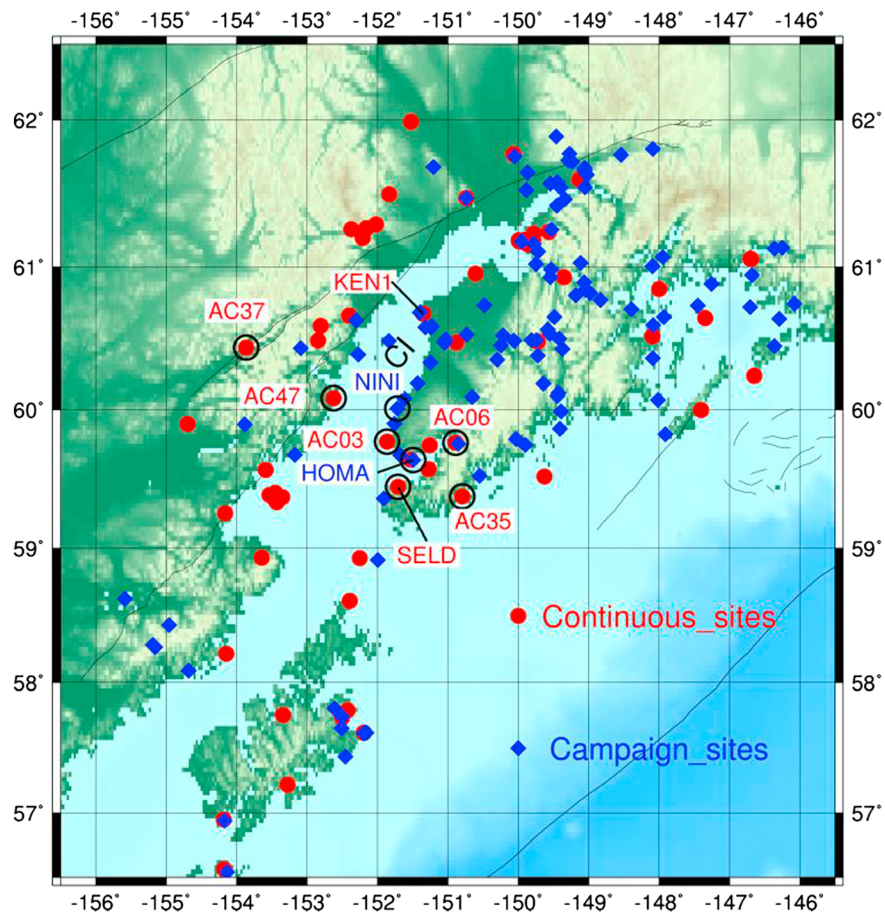


**Figure 2.** Continuous (red) and campaign GPS sites in the study area. The sites SELD and KEN1 are labeled, and the other sites shown in Figure 3a are circled with outlines and also labeled.

subduction zone. The 1964 earthquake ( $M_w$  9.2) [Cohen and Freymueller, 2004] ruptured the eastern section of the subduction zone (purple outline in Figure 1), and its postseismic deformation continues today [Suito and Freymueller, 2009].

### 1.3. Previous Work

Slow slip events (SSEs) with durations from days to years have been observed in many subduction zones. The largest SSEs on the Cascadia subduction interface last days to weeks and are estimated to have ~2 cm of aseismic slip over the interface downdip from the seismogenic zone and moment magnitudes of ~6.7 [Dragert *et al.*, 2001; Szeliga *et al.*, 2004]. These and all other magnitudes in this paper are estimated from geodesy, and the moments depend on the assumed shear modulus; we assume 50 GPa for the Lower Cook Inlet event. Kostoglodov *et al.* [2003] observed a large SSE in southern Mexico lasting about 6–7 months in the Guerrero seismic gap, with average slip of ~10 cm and a moment magnitude of ~7.5. Several short-term and long-term slow slip events were observed in southwest and central Japan. For example, a long-term SSE occurred in the Tokai region from 2000 to 2005 with the maximum slip rate about 20 mm/yr faster than plate motion rate (overslip) and a moment magnitude of  $M_w$  ~6.6 [Ochi and Kato, 2013]. Some short-term slow slip events have been detected along the Nankai Trough in southwest Japan with moment magnitudes ranging from 5.5 to 6.3 [Nishimura *et al.*, 2013]. At least 15 SSEs have occurred at the Hikurangi subduction margin since 2002; the durations of these events varied from 6 days to 1.5 years with moment magnitude ranging between  $M_w$  6.3 and 7.2 [Wallace and Beavan, 2010].

In Alaska, Ohta *et al.* [2006] discovered a large slow slip event from 1998 to 2001 below Upper Cook Inlet within the south central Alaska subduction zone. Fu and Freymueller [2013] identified a second slow slip

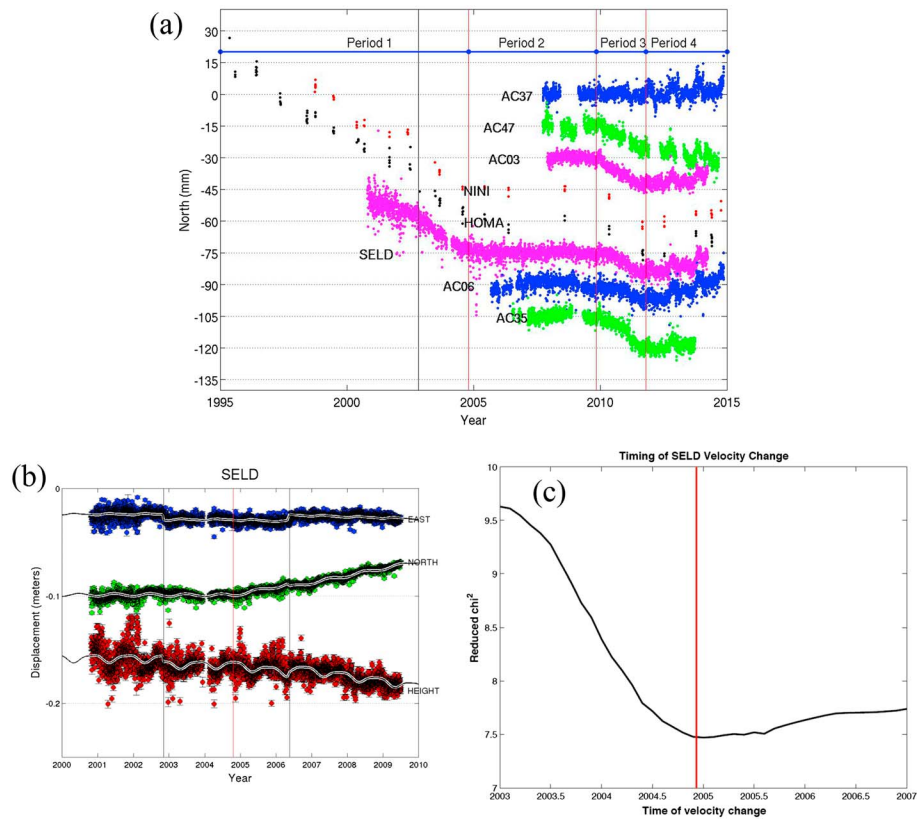


**Figure 3.** (a) North components of time series (detrended using the average velocity in 2004–2010) from a sample of GPS stations, ordered in a trench-normal profile (black outlines in Figure 2). Red lines show the dates of velocity changes. The 2002 Denali Fault earthquake (black solid line) caused an offset at these sites but mainly in the east component (not shown). The east component shows much smaller changes in trend than the north component. Period 1: 1992–~2004; period 2: ~2004–~2010; period 3: ~2010–~2011; and period 4: ~2011–~2015. (b) Seldovia (SELD) time series used for estimation of timing of the velocity change at about 2004, detrended based on pre-2004.8 data. The red line shows the estimated time of the velocity change, while the black lines show the times of offsets. The black-white curve shows the estimated model fit to the time series. (c) Estimation of timing of SELD velocity change at 2004.8. The reduced chi-square of the least squares fit is plotted as a function of the assumed time of the velocity change. The best fit timing of the velocity change is shown by the red line.

event from 2008.96 to 2012.87 in the same area as the 1998–2001 SSE, and Wei *et al.* [2012] identified another SSE that occurred beneath the Lower Cook Inlet from 2010 to 2011 located southwest of the 1998–2001 SSE.

#### 1.4. Present Study

We relate the observations of abrupt changes in GPS site motions in late 2004, ~2010, and ~2011 around the Lower Cook Inlet region to changes in the slip distribution on the plate interface.

We augment the sparse continuous GPS data from 1996 to 2014 with repeat surveys of campaign GPS sites starting in the 1990s to the end of 2014 to better estimate the velocity changes. As described below, we divide the GPS time series into four time periods based on the observed changes in trends at ~2004, ~2010, and ~2011. Using the horizontal components of the GPS velocities, we estimate the slip variations below the Lower Cook Inlet of the Alaska-Aleutian subduction zone for each period and then evaluate whether they indicate the occurrence of slow slip events or changes in the extent of the locked zone. Meade and Loveless [2009] proposed that very long duration SSEs would have slip rates comparable to plate motion rates, which would make them difficult to distinguish from partial locking. However, rates of slip on the interface faster than plate motion, aside from postseismic transient effects, can only result from SSEs. Therefore, we assume that the presence of overslip as described above requires an SSE.

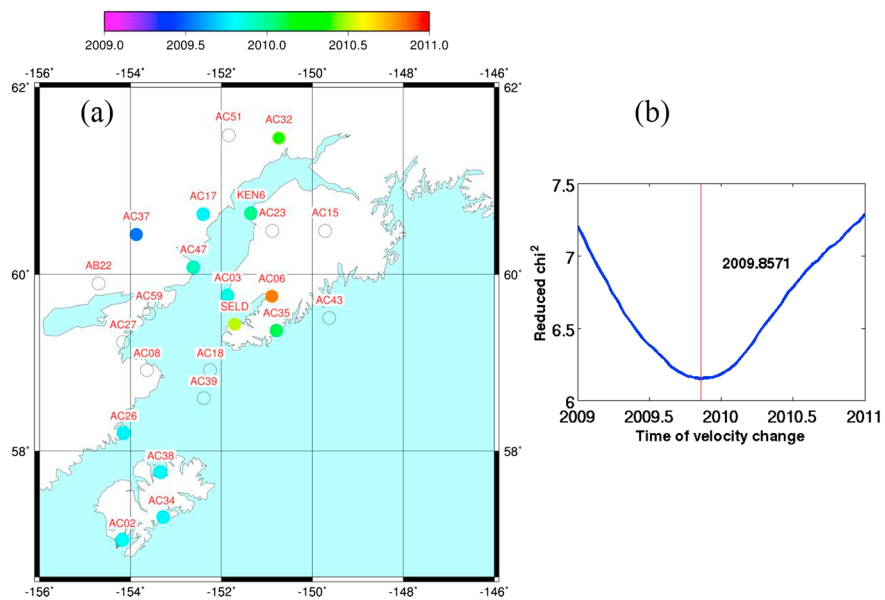


**Figure 4.** (a) The spatial distribution of timing of velocity change for the continuous sites and (b) the general result for timing of velocity change at  $\sim 2010$  based on absolute difference of misfit for significant sites.

## 2. GPS Data and Analysis

### 2.1. GPS Data and Characteristics of the Time Series

We estimate the slip deficit distribution on the plate interface and its time dependence by using 65 continuous and 107 campaign GPS sites in total (Figure 2). GPS sites located on or near active volcanoes were not used.

We use the GIPSY/OASIS goa-5.0 software developed by Jet Propulsion Laboratory (JPL) to obtain daily coordinate and covariance estimates for all the GPS continuous and campaign stations around the Cook Inlet region. We adopt the JPL nonfiducial orbits and clock products, derived from a free network solution, and estimate a daily transformation for each solution into the ITRF2008 reference frame. The details of the data analysis were described in *Fu et al. [2012]*.

The GPS time series reveal abrupt changes in slopes (velocities) in Lower Cook Inlet of the Alaska-Aleutian subduction zone in late 2004, early 2010, and late 2011 (Figure 3a). There were only two continuous GPS sites operating in the area prior to 2004. Site SELD in Seldovia (Figure 2), set up in 2000 (Figure 3b), reveals a velocity change in the north component at about 2004 (Figures 3b and 3c). A small offset in the east component at  $\sim 2006.4$  is due to an antenna change. The north components of the time series of several other continuous and campaign sites around the study area (examples shown in Figure 3a) also reveal velocity changes at  $\sim 2010.0$  and  $\sim 2011.0$ . Relative to the 2004.8–2010 velocities, sites in the study area generally moved faster southward prior to 2004.8 and did so again from early 2010 to late 2011 (Figure 3a). Post-2011 motions are similar to those of 2004.8–2010 or are slightly more northward. Site KEN1 in Nikiski (Figure 2) has a similar timing of velocity change as SELD, but the change is smaller, and including KEN1 does not improve the estimate of the timing. The timing of the velocity changes is examined in the following section.

### 2.2. Estimating Timing of Velocity Change

To estimate the timing of the velocity change in late 2004, we first detrend the time series from SELD (Figure 3b) based on the pre-2004 velocity. It is evident that the site moved faster to the north after late 2004. We then fit the time series assuming an abrupt velocity change, as well as offsets in 2002 for the Denali Fault earthquake and in 2006 for a receiver/antenna change. We test a series of dates for the timing of the velocity change by least squares fit to the positions. There is a broad minimum in the misfits between mid-2004 and mid-2005 (Figure 3c), while the minimum is at 2004.8. The pattern of the velocity changes is consistent with an expansion of the downdip width of the locked zone on the plate interface after

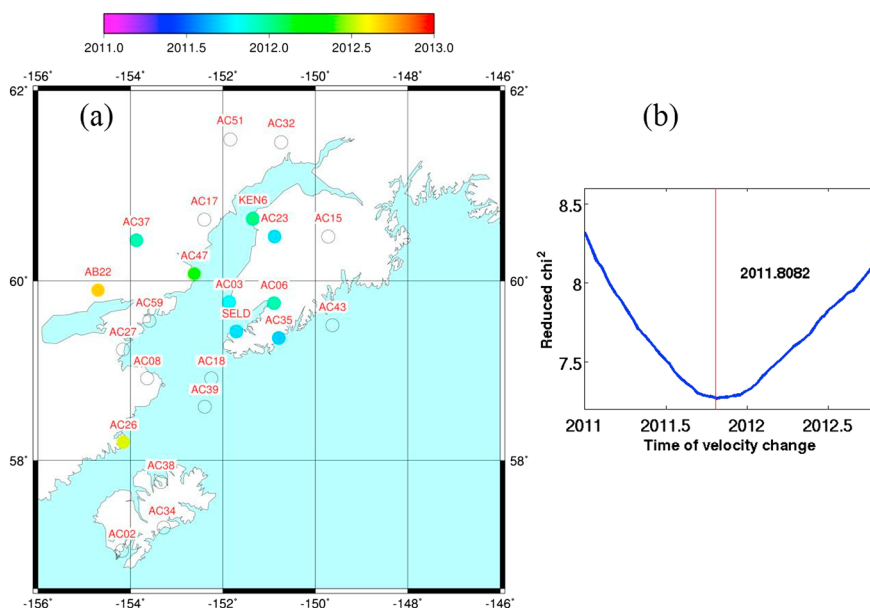


**Figure 5.** (a) The spatial distribution of timing of velocity change for the continuous sites and (b) the general result for the timing of velocity change at  $\sim 2011$ .

$\sim 2004.8$ , as it is the elastic deformation from the locked zone that causes motion in a roughly northward direction here.

To estimate the specific timing of velocity changes in  $\sim 2010$  and  $\sim 2011$ , we use the time series from 23 continuous sites around Lower Cook Inlet and the same approach described above for SELD. Unlike for the 2004.8 change, the test for the timing of the velocity change reveals a narrow minimum in the misfit for each individual site. However, when all sites are combined, the minimum in the misfit is broader because the specific date of the velocity change varies from site to site, likely due to migration of the slip on the plate boundary. Therefore, we fit each site independently and use only those sites that have significant changes in velocity to estimate the best time to use. We test thresholds based on three different criteria of significance of the velocity change: the relative difference of the data misfit, the absolute difference of data misfit, and the magnitude of velocity change. We find that the second criterion, the absolute difference of the misfit, produces the most spatially coherent set of sites with significant changes (Figures 4, S1 in the supporting information, and 5).

After removing the sites that show no significant velocity change based on each of the criteria, we map the spatial distribution of the timing of the velocity changes (Figure S1). For the change at  $\sim 2010.0$ , it appears that the velocities of sites over deeper parts of the plate interface (downdip) changed first and then the sites to the SE (updip) changed later (Figure 4a). Based on the selected significant sites (Figure 4), the mean timing of velocity change at  $\sim 2010$  is at 2009.85.

We apply the same approach for estimating the timing of velocity change in 2011 and find the average of 2011.81 (Figure 5). For this velocity change, the updip sites changed first and then the velocity change gradually propagated toward the downdip sites, opposite the direction of propagation in early 2010.

### 2.3. GPS Velocities

Based on the estimates of the velocity changes in late 2004,  $\sim 2010$ , and late 2011 as determined above, we divide the GPS time series into four time periods: period 1 (1992.0–2004.8), period 2 (2004.8–2009.85), period 3 (2009.85–2011.81), and period 4 (2011.81–2014.87). For almost all sites, the data span used by *Suito and Freymueller [2009]* is the same as our period 1 because there were only a few campaign measurements made between 2004 and 2009.

We use only the horizontal GPS velocities for estimating the interseismic slip distributions because of the high uncertainties in the vertical component and large vertical deformation due to glacial isostatic adjustment

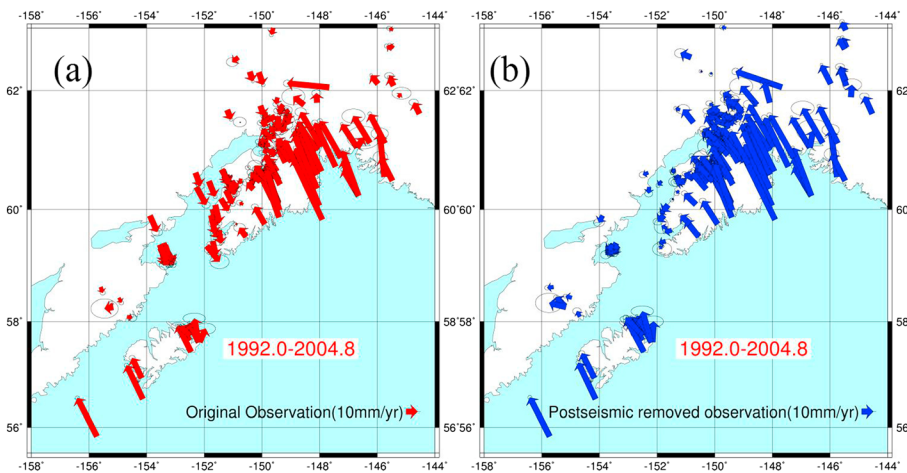


**Figure 6.** Comparison between (a) original GPS velocity data and (b) GPS velocity data with postseismic effect corrected for period 1: 1992.0–2004.8 (Figures 6a and 6b).

(GIA). We calculate GPS velocities from individual site time series by weighted least squares using all data from each period and correct the velocities for the estimated geocenter translation rate of the ITRF2008 based on *Altamimi et al.* [2011]. Then we remove the motion of North America in ITRF2008 to transform velocities into a North America fixed reference frame [*Argus et al.*, 2010] and apply GRACE-derived seasonal variation corrections [*Fu et al.*, 2012] to the continuous and campaign GPS time series.

The GPS velocity field reveals strong along-strike and across-strike gradients [*Suito and Freymueller*, 2009]. Outside of the Cook Inlet region, the velocity fields for all four time periods are similar, differing mainly in the sites available. Velocities close to Prince William Sound are generally higher than those on the Kenai Peninsula. The sites far from the trench tend to move trenchward, while the sites closer to the trench move in the direction of relative Pacific Plate motion (Figure 6). Postseismic deformation from the 1964 earthquake causes the trenchward motion, while elastic deformation from locking on the subduction interface causes motion in the direction of plate motion [*Suito and Freymueller*, 2009]. We remove the postseismic deformation using the model of *Suito and Freymueller* [2009] to isolate the interseismic deformation. We minimize the effect of postseismic deformation from the 2002 Denali earthquake by using only sites located well to the south of the Denali Fault. This selection is based on the predictions of existing postseismic models [*Freed et al.*, 2006; *Johnson et al.*, 2009], which predict negligible postseismic displacements in our study region, except for the northwest corner.

Figure 6 shows the comparison between original GPS velocities and GPS velocities with postseismic deformation removed for period 1 (a and b). The same information for periods 2–4 is shown in Figure S2 in the supporting information. The trenchward postseismic motion from the original velocity field disappears when the postseismic model is subtracted from the data, especially in the west and northwest parts of the study area.

### 3. Modeling Approach and Evaluation

#### 3.1. Block Model

The entire upper plate in the southern Alaska subduction zone moves relative to North America [*Freymueller et al.*, 2008], and we must account for this motion via a block model to avoid biasing the estimated slip distribution on the megathrust. Estimating the motion of all of the upper plate blocks would require using GPS velocities from a much larger area and accounting for additional complications that are not relevant to the main topic of this paper. Therefore, we first develop a block model using mostly published sources and keep that model fixed for investigation of the time dependence of slip on the plate interface.

*Lahr and Plafker* [1980] proposed a model for the tectonics of southern Alaska comprising three blocks: the Wrangell block, the St. Elias block, and the Yakutat block. Relative motion rates in their model were educated guesses, which turned out to agree fairly well with later geodetic data [*Freymueller et al.*, 2008]. *Fletcher* [2002]

**Table 1.** Block Poles, Location of Poles, and Angular Speed of the Block Model, Relative to the North American Plate<sup>a</sup>

Block Name	Latitude of Pole	Longitude of Pole	Angular Speed (deg/Ma)	Source
SOAK	59.6000	212.6002	0.7700	Fletcher [2002]
PCFC	50.1734	284.1136	-0.7696	Sella <i>et al.</i> [2007]
BRNG	43.9007	125.6082	-0.0638	Cross and Freymueller [2008]
PENN	60.481	58.666	-0.066	This study (section 3.2)

<sup>a</sup>Negative rotations are clockwise looking from above.

improved the *Lahr and Plafker* [1980] relative block motion rates based on the GPS data available at that time but used different block names: the southern Alaska block (SOAK) instead of the Wrangell block and the Fairweather block instead of the St. Elias block. In Fletcher [2002], the pole of rotation for SOAK relative to the North American Plate (NOAM) was based on the fit of a small circle to the trace of the central Denali Fault. The angular speed of the SOAK block (Table 1) was calculated by estimating the average slip rate on the Denali Fault from the available GPS data at that time [Fletcher, 2002; Freymueller *et al.*, 2008].

*Cross and Freymueller* [2008] discovered that sites in western Alaska and on the Bering Sea Islands have southward or southwestward velocities relative to NOAM. These velocities were well fit by a single clockwise rotation about a pole located in northeast Asia. They called this block the Bering plate (BRNG), although they could not define its eastern boundary (Figure 1), and proposed that the Alaska Peninsula lay on the Bering plate. *Suito and Freymueller* [2009] suggested that the systematic residuals of sites on the Kenai Peninsula relative to the interseismic model result from westward block motion relative to both SOAK and NOAM. These residuals are similar to the motion of sites on the Alaska Peninsula from *Cross and Freymueller* [2008]. Given that and the lack of a clear tectonic boundary between the Alaska Peninsula and the Kenai Peninsula, we test a model with an additional Peninsula block (PENN) that includes both regions. Our model uses the SOAK block from Fletcher [2002], BRNG [*Cross and Freymueller*, 2008], the PENN block, and two major plates: NOAM and the Pacific Plate (PCFC) [Sella *et al.*, 2007] (Figure 1). We estimate the angular velocity of PENN but fix the poles of all the other plates and blocks at their published values (Table 1). We also test a recently published PCFC-NOAM pole [DeMets *et al.*, 2014]. That pole produces a slower convergence rate at the Alaska trench, and the model residuals approximately double if we use it in place of the Sella *et al.* [2007] pole because the observed strain in the upper plate cannot be matched even with a wide fully locked interface. Therefore, we use the estimate from Sella *et al.* [2007] in this paper.

### 3.2. Estimation of Angular Velocity of PENN Block

We estimate the pole of rotation of the Peninsula block (PENN) by using GPS sites in periods 1 and 4 because there are more sites with precise velocities in period 1 (due to its long duration), and period 4 has the second best distribution of sites and the most continuous sites. Compared with periods 1 and 4, period 2 has very few campaign sites, and period 3 spans only 2 years (resulting in large uncertainties). We find that the data from these latter two time periods are consistent with the angular velocity of PENN estimated from periods 1 and 4.

The subducting plate geometry beneath southern Alaska is complex due to the transition from Pacific Plate subduction to Yakutat terrane collision. Brocher *et al.* [1994] suggested that there were actually two separate subduction interfaces beneath Prince William Sound: Yakutat subducting beneath North America and Pacific subducting beneath Yakutat. In this paper we use the Slab 1.0 plate geometry [Hayes *et al.*, 2012], which is considerably deeper (by as much as 15–20 km beneath Upper Cook Inlet) than the slab geometry assumed in previous studies [*Suito and Freymueller*, 2009]. The slab geometries are more similar in Lower Cook Inlet and are essentially the same from Kodiak Island to the west. Assuming a shallower plate interface would reduce the estimated magnitude of slip in the slow slip events because the interface is shallower (less slip is needed to cause the same deformation at the surface), but for this study we retain Slab 1.0 because it is not yet clear which geometry is more accurate.

After removing the 1964 earthquake postseismic effect from the horizontal GPS velocities, they can be expressed as a combination of block rotations and the elastic deformation from locked faults, including the Denali Fault and the subduction megathrust. We perform a nonlinear, constrained, least squares inversion to estimate the pole of rotation of the PENN block and the plate locking variation simultaneously using a simulated annealing approach [Press, 1989] in the program TDEFNODE [McCaffrey, 2009]. All other block

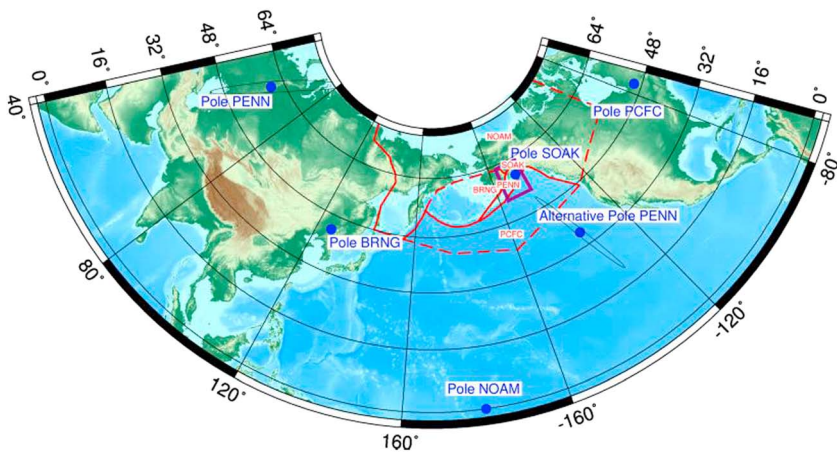


**Figure 7.** The location of poles (blue dots) for all the blocks. The red solid and dashed lines show the block boundaries. The purple rectangle shows the main study area. The alternate pole for PENN, based only on data from the main study area, is located in the eastern Pacific.

angular velocities are fixed to the values in Table 1. Details of the block boundaries will be described in section 3.3. The site velocity is equal to

$$v_i(x_{\text{site}}) = v_B - v_{SD} = \Omega \times x_{\text{site}} - v_{SD} \quad (1)$$

$v_B$  is the velocity at the site due to block rotation,  $v_{SD}$  is the surface velocity related to the fault slip deficit distribution,  $x_{\text{site}}$  is the vector pointing from the Earth's center to the surface observation point, and  $\Omega$  is the angular velocity of the block that contains the site relative to the reference plate NOAM. The slip deficit rate on the megathrust is parameterized using a spatially variable coefficient  $\phi$ , multiplied by the relative plate velocities determined from the block angular velocities projected onto the fault plane. The details of the calculation approach of TDEFNODE are given in McCaffrey [2002] (<http://web.pdx.edu/~mccaf/www/defnode>).

We estimate the angular velocity of the PENN block based on the approach outlined above by using three different velocity sets: period 1 only, period 4 only, and a combination of periods 1 and 4. In the solution using the combination, we use the average velocity and its corresponding uncertainty if a site was present in both time periods. All three inversions produce a similar solution for the PENN block, so we adopt the solution for the angular velocity of the PENN block (Table 1) estimated from the combination of GPS velocities from periods 1 and 4. We use data from our main study area and also from the Alaska Peninsula; see Figure S3 for the observations and model predictions from this inversion. Figure 7 shows the location of poles for all the blocks in the block model. The estimated block rotation velocities for sites on the PENN block have clear southwestward motion (Figure 8). For the remainder of this paper, we will keep the angular velocity of PENN fixed while we estimate the slip deficit distributions.

The location of the pole for the PENN block is quite sensitive to small changes in the data used in the inversion, although the predicted block motion velocities are not. The best fit pole for the PENN block is located in northern Russia, but if we use data only from the main study area (Cook Inlet), then the pole shifts to a location south-southeast of Alaska, in the Pacific Ocean (Figure 7). A great circle connecting these two poles passes through the center of the PENN block itself, and both poles give nearly identical trench-parallel velocities over the limited area of the PENN block (one pole has clockwise rotation and the other counterclockwise). There are small differences in the trench-normal motions predicted by these two poles, but only about 0.5 mm/yr, and the small difference changes the estimated slip distribution only slightly. Therefore, the predicted block motions are well determined even if the pole of rotation is not, and we use the PENN pole based on the larger data set.

### 3.3. Modeling of Slip Deficit Rate Distribution

We use TDEFNODE [McCaffrey, 2002, 2009] to estimate the block-bounding fault slip deficit rate distributions for each time period by inverting the GPS velocity data. We then interpret variations in the slip deficit rate

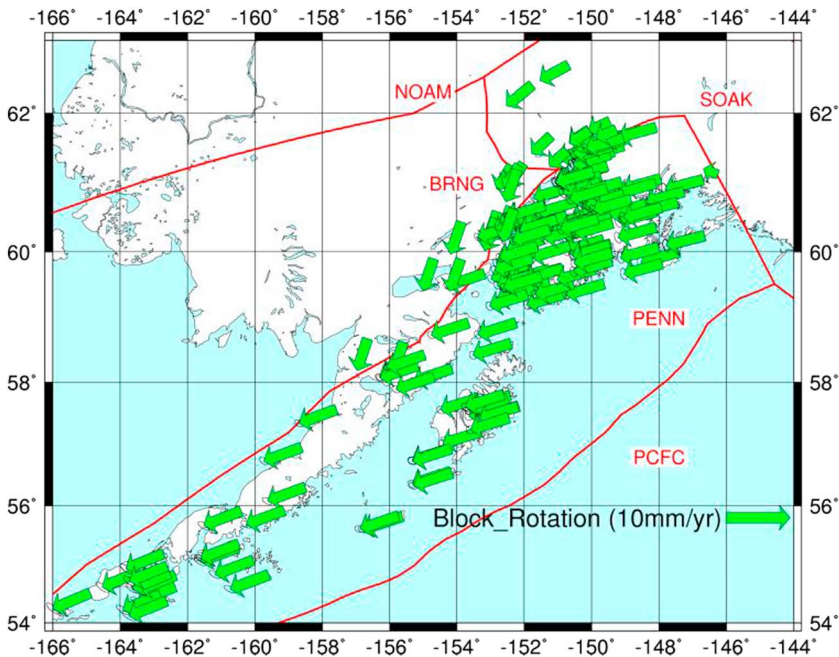


**Figure 8.** Predicted rotation velocities based on the pole estimated by inversion of the combination of data from periods 1 and 4. Red solid lines show the block boundaries. Sites on the Kenai Peninsula and Alaska Peninsula move almost uniformly toward the southwest.

distribution in terms of locking variations and transients such as slow slip events. For these inversions, we fix the block motions per Table 1.

TDEFNODE combines spherical block rotations with interseismic locking distributions on the faults using the half-space dislocation method [Okada, 1985]. The main faults that define boundaries in the model are the central Denali Fault and the Aleutian subduction zone based on mapped fault segments. All blocks must be closed polygons, and arbitrary boundaries were used far from the data used here to do that. The subduction zone geometry is based on Slab 1.0, a three-dimensional representation of the Alaska-Aleutian subduction zone [Hayes et al., 2012] (Figure 1). The Aleutian slab geometry based on Slab 1.0 is digitized about every 35 km in the along-strike direction and about every 5 km in the downdip direction. The locations of the irregular grid of nodes on the fault surface are specified by their latitude, longitude, and depth producing a continuous fault geometry. The coupling fraction  $\phi$  (ratio of the slip deficit rate to the long-term slip rate) is estimated at each node subject to spatial smoothing as described below. The fault slip rate and rake are determined by the relative block motions, so the single parameter  $\phi$  fully accounts for the slip deficit rate.

We place bounds on the allowed values of  $\phi$  (slip deficit fraction) and estimate the slip deficit distribution subject to additional smoothing constraints. Negative values of  $\phi$  imply an excess of slip (overslip), where the slip rate exceeds the plate motion rate and would indicate the presence of a slow slip event. Slip rates during SSE at other subduction zones can be many times the plate convergence rate. For example, in Cascadia a typical average rate is about 500 mm/yr ( $\sim 1$  cm/week) which is more than 10 times the convergence rate. To find out whether or not negative slip deficit rates are required in our region, we apply several different bounds on the coupling ratio  $\phi$ :  $[-100, 1]$  (Figure S4a),  $[-2, 1]$  (Figure 11a),  $[-1, 1]$  (Figure S4b), and  $[0, 1]$  (Figure 11b) where the brackets indicate minimum and maximum values allowed. Comparing the slip distributions from these different  $\phi$  ranges (Figure S4), we find that minimum slip deficit rate in the setting of  $\phi [-100, 1]$  was almost the same with the one obtained by restricting  $\phi$  to the range  $[-2, 1]$  for all reasonable amounts of smoothing. The minimum  $\phi$  value from  $\phi [-2, 1]$  tended to be smaller than the one from  $\phi [-1, 1]$ , although differences in these slip distributions are mainly in areas of poor model resolution. We also find that  $\phi$  values observed in other SSEs in Alaska [Ohta et al., 2006] were close to  $-1$ . Therefore, a  $\phi$  range of  $[-2, 1]$  allows for reasonable slip rates for the long-term SSEs observed here. In addition to fixing the allowable  $\phi$  range as  $[-2, 1]$ , we also fix the coupling ratio to 0 at the deepest nodes (deeper than 70 km) on the

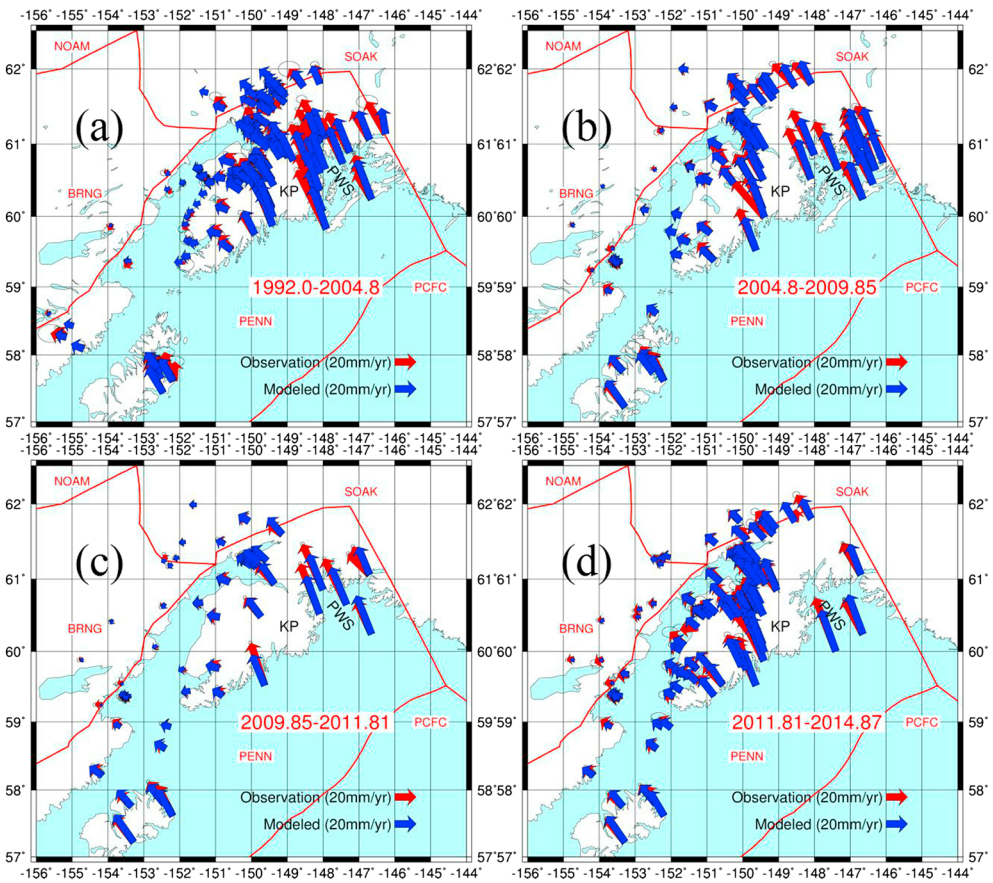


**Figure 9.** Comparison between the predicted (blue) and observed (red) velocities for each time period. (a) Period 1 (1992.0–2004.8), (b) period 2 (2004.8–2009.85), (c) period 3 (2009.85–2011.81), and (d) period 4 (2011.81–2014.87). PWS: Prince William Sound and KP: Kenai Peninsula.

fault because we assume that a fully slipping state occurs at these depths.  $\phi$  values at the shallowest nodes are not constrained. We use a starting value of 0 for all  $\phi$  values.

The estimation of the slip distribution as we pose it is mixed determined, so we apply Laplacian smoothing with the same smoothing factors in both the along-strike and downdip directions. We find the optimal trade-off between the data misfit based on the weighted residuals  $\mathbf{r}^T \cdot \mathbf{W} \cdot \mathbf{r}$  and the model roughness defined by Laplacian of the slip distribution and minimize the sum of these two quantities  $F$  (equation (2)).

$$F = \mathbf{r}^T \cdot \mathbf{W} \cdot \mathbf{r} + \frac{A \left( \frac{\partial^2 \phi}{\partial x^2} + \frac{\partial^2 \phi}{\partial w^2} \right)}{n} \quad (2)$$

The first term in equation (2) includes the residual  $\mathbf{r}$ , and  $\mathbf{W}$  is the weight matrix, the inverse of the data covariance matrix. The second term will be called the roughness of the model, where  $A$  is the smoothing factor (weight) for both along-strike and downdip directions,  $\phi$  is the locking fraction,  $x$  is along strike,  $w$  is along the dip direction, and  $n$  is the number of free nodes on the fault surface. Varying the smoothing factor  $A$  generates a series of solutions where the curvature of the locking pattern is damped (Figure S4). After analyzing the trade-off curves for each time period, we find that the optimal ranges of the smoothing factor are similar for all four time periods. Thus, we choose the same preferred smoothing factor for four time periods,  $A = 1 \cdot 10^7$ .

## 4. Results

### 4.1. Model Prediction Versus Observed Velocity Data in the Four Time Periods

For each time period, we fix the angular velocities of all blocks and estimate the fault slip deficit distributions using TDEFNODE, with the slab geometry and smoothing given in the previous section. Figure 9 shows the

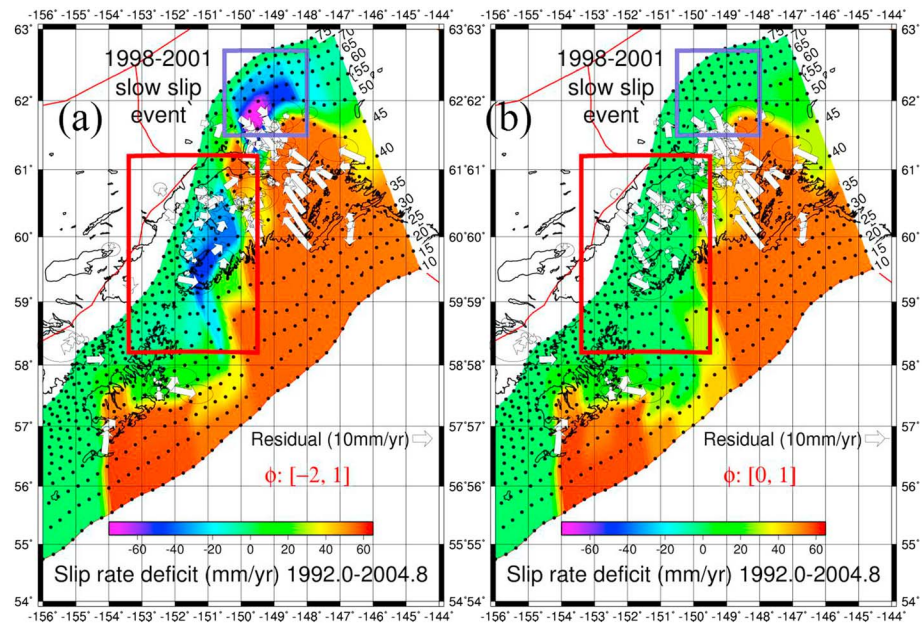


**Figure 10.** Slip deficit rate distribution and residual of GPS velocities (white arrows) with the node geometry for (a)  $\phi$  in the range  $[-2, 1]$  and (b)  $\phi$  in the range  $[0, 1]$  during period 1 (1992.0–2004.8). The red box marks the region affected by the temporal changes in slip deficit. Contours including black points (nodes) show the depth of the subduction zone. The blue box marks the area where displacements from the 1998–2001 slow slip event are large, based on Ohta et al. [2006].

observed and calculated GPS velocities for each time period using the  $\phi$  range  $[-2, 1]$ . The model fits the velocities well, in general, except for within Prince William Sound (for all time periods). The residuals in Prince William Sound will be discussed at the end of the next section.

#### 4.2. Slip Distribution in Each Time Period

We estimate locking for each time period with two different limiting ranges of the locking fraction ( $\phi$ ):  $[-2, 1]$  and  $[0, 1]$ . Slip rates faster than the plate convergence rate ( $\phi < 0$ ) are interpreted as slow slip events, while  $\phi$

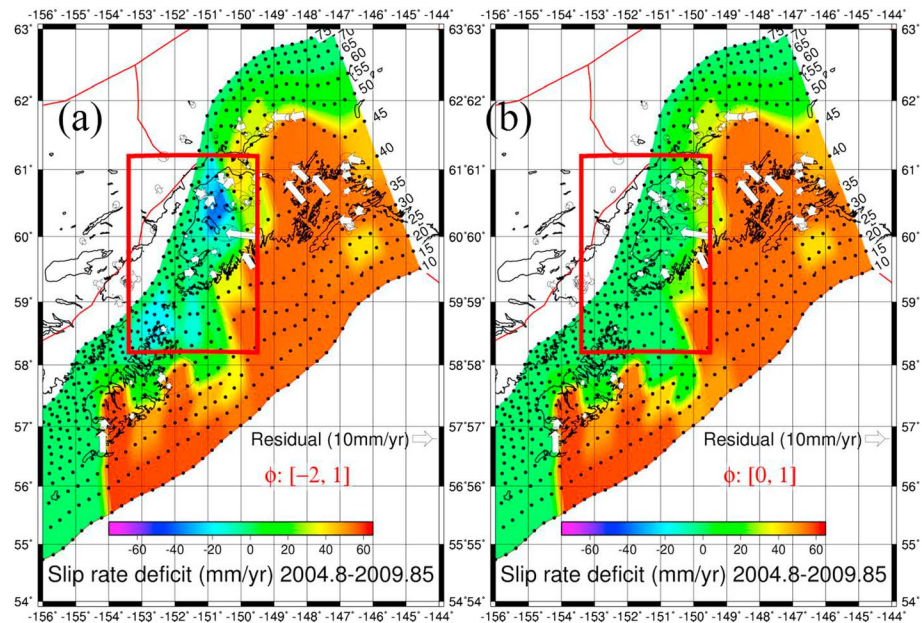


**Figure 11.** Slip deficit rate distribution and residual of GPS velocities with the node geometry for (a)  $\phi$   $[-2, 1]$  and (b)  $\phi$   $[0, 1]$  during period 2 (2004.8–2009.85). The red box, arrows, and contours are the same as in Figure 10.

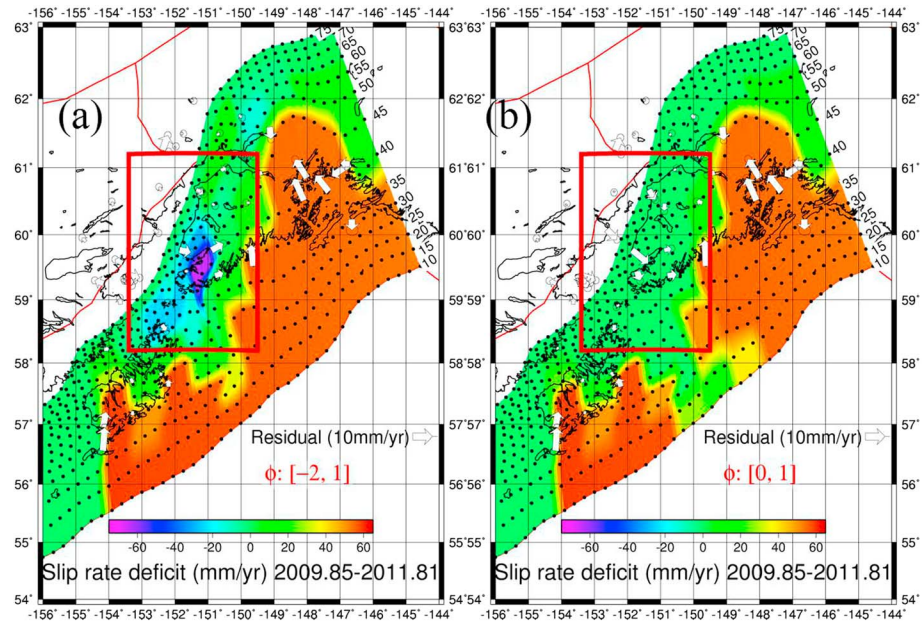


**Figure 12.** Slip deficit rate distribution and residual of GPS velocities with the node geometry for (a)  $\phi$  [-2, 1] and (b)  $\phi$  [0, 1] during period 3 (2009.85–2011.81). The red box, arrows, and contours are the same as in Figure 10.

values that change but remain positive may correspond to SSE or temporal changes of the locking. Figures 10–13 show the fault slip deficit distributions and residuals for both ranges of  $\phi$  for each time period. The distribution of slip deficit is similar in all time periods for the shallow parts of the fault (at least below the areas where there are data and hence resolution). However, while the first-order pattern is similar through time, there are large differences between the periods at the downdip limit of the locked region. To test whether slip rates faster than the plate convergence rate are required to satisfy the data, we calculate and compare the sum of squares of the weighted residuals (variance) between the two different solutions for each time period, using data from the sites in the area that shows a significant change in the slip deficit rate

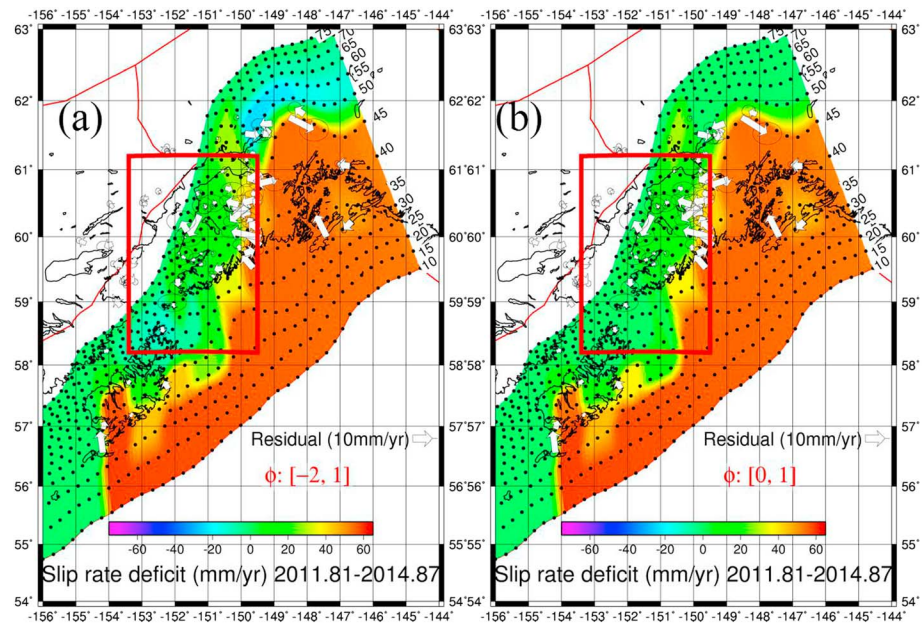


**Figure 13.** Slip deficit rate distribution and residual of GPS velocities with the node geometry for (a)  $\phi$  [-2, 1] and (b)  $\phi$  [0, 1] during period 4 (2011.81–2014.87). The red box, arrows, and contours are the same as in Figure 10.

**Table 2.** The Variance for the Selected Boxes in Four Time Periods<sup>a</sup>

	The selected box/region	$\phi: [-2, 1]$	$\phi: [0, 1]$	Difference
1992.0–2004.8	blue box	1175.66	1931.86	756.19
1992.0–2004.8	red box	1227.09	1972.95	745.86
2004.8–2009.85	red box	441.932	529.613	87.6810
2009.85–2011.81	red box	307.33	536.72	229.39
2011.81–2014.87	red box	907.615	971.264	63.6490

<sup>a</sup>All variances have units of (mm/yr)<sup>2</sup>.

(Table 2). The differences in misfit when the bounds on  $\phi$  were changed were large for periods 1 and 3 but small for periods 2 and 4.

Based on the residual variance in the same selected area (red box in Figures 10–13), negative slip deficit rates identified in period 1 (1992.0–2004.8) and period 3 (2009.85–2011.81) fit better compared to a model with only positive slip deficit rates. For periods 1 and 3, the variances of residuals are reduced by about 64% and 74%, respectively, by allowing negative  $\phi$  values in the red box area (Figures 10–13). For the other two time periods, the differences in variance are much smaller, which are both less than 20%. For this paper, we consider the >50% reduction in misfit for periods 1 and 3 to be significant, requiring that slip on the interface exceeded the rate of plate motion. This significant overslip requires the occurrence of slow slip events during period 1 and period 3 [Ochi and Kato, 2013]. The Lower Cook Inlet slow slip event during period 1 lasted at least 9 years, given that our observations in that area began in 1995, and the pattern of site velocities was nearly constant from 1995 to 2004. We discuss the long duration of the slow slip event, the slip distribution pattern, and locking distribution on the fault in section 5. For periods 2 and 4, allowing slip to be faster than plate motion does improve the fit to the data, but the improvement is much less convincing in the Lower Cook Inlet area. In particular, in period 4 the improvement in misfit in the Lower Cook Inlet area is only 7% if we allow slip faster than plate motion.

The blue box in Figure 10, outlining the area of the known 1998–2001 Upper Cook Inlet SSE, is drawn based on the model of Ohta *et al.* [2006]. The time periods chosen in this study are based on the observed changes in motion in Lower Cook Inlet, which are not synchronous with the SSEs in Upper Cook Inlet. For example, the 1998–2001 SSE lies within our period 1 but is averaged together with an equal or greater length of time with no SSE. As a result, we do not recover the full amplitude of the SSE. The later 2009–2013 SSE [Fu and Freymueller, 2013; Fu *et al.*, 2015] is divided across three of our time periods, and as a result it has almost no impact on period 2 and a reduced impact on period 4, which includes 2 years of data after the SSE. It can still be clearly seen in Figures 12a and 13a. An inversion for a time series of slip deficit based on the GPS time series, rather than velocities, will be needed to study both regions at the same time and to assess the temporal relationship between nearby events more fully.

Observed velocities near Prince William Sound are systematically underpredicted for all time periods even though  $\phi$  is at its maximum value (fully locked) in this area. We test two alternate models to evaluate two possible explanations for these systematic residuals: (a) our assumed plate geometry is too deep and (b) the sites in Prince William Sound lie on a block separate from PENN. The region just to the east of our study area has several upper plate blocks [Elliott *et al.*, 2013], but none of them can explain the residuals. Making the subduction geometry shallower using the geometric model of Suito and Freymueller [2009] decreases the misfit in Prince William Sound by ~24% but results in only small changes elsewhere (this model of the plate interface is as much as 10–15 km shallower than Slab 1.0 along a cross section passing through Prince William Sound). Adding a new block for Prince William Sound produces a larger improvement in the misfit in that area, ~35%, but again very small changes in the model elsewhere. Adding a block for Prince William Sound does not change the estimated slip deficit distribution except immediately over Prince William Sound, but making the plate interface much shallower reduces the size of the estimated locked area, in general, and reduces the magnitude of inferred forward slip in the slow slip events. We retain the original geometry and block model for the results shown here, but note that the inferred moment magnitudes of all SSEs in the region from this study [Wei *et al.*, 2012; Fu and Freymueller, 2013] might be overestimates if the active plate interface is much shallower than Slab 1.0.

#### 4.3. Model Resolution

To reveal the sensitivity and resolution of our inversion method, we conduct a synthetic checkerboard test. We run a forward model with starting  $\phi$  values of either 1 or 0 in a checkerboard pattern (Figure S5a) and

add random errors with the same variance as those of the observed velocities to the calculated velocities at each site. We then invert the synthetic data using the same inversion settings as our best inversion models. The recovered model (Figure S5b) reproduces the test model well for the area where GPS stations are most dense, on land and immediately offshore. Model resolution is good for the Lower Cook Inlet area but minimal in the near-trench region. The original model is recovered faithfully for the region of slow slip, at the downdip end of the locked zone. The lack of resolution near the trench, and offshore, in general, is not surprising given the long distance from the shoreline to the trench. However, the onshore part of the seismogenic zone is resolved well.

## 5. Discussion

### 5.1. Interseismic Slip Deficit Distribution and Reconstruction of Slip History Over the Last 20 Years

The slip deficit rate distribution for period 1 based on  $\phi$  in the range  $[-2, 1]$  in Figure 10 shows two significant patches of overslip: one is below the Upper Cook Inlet area, known to be the area of a large 1998–2001 SSE [Ohta et al., 2006], and the other one is mainly over the depth range of 36–60 km in the Lower Cook Inlet area. These two overslip patches indicate two separate SSEs during period 1. Figure 12 shows the slip deficit rate distribution for the two different  $\phi$  ranges for period 3, which indicates an area of overslip over the depth range of 36–56 km in the Lower Cook Inlet area, also presumed to be an ~2 year long SSE [Wei et al., 2012]. Period 2 (Figure 11) has a small area of overslip in Lower Cook Inlet, in the same place as the SSE in period 1, which could be a remnant of that SSE. However, the model in which only positive slip deficit is allowed only increases the misfit by 20%, so the evidence for slip faster than plate motion is less clear than for periods 1 and 3. Period 4 (Figure 13) has no active SSE in Lower Cook Inlet, but a clear area of overslip in Upper Cook Inlet, which is the SSE identified by Fu and Freymueller [2013]. The slip deficit rate distribution in period 4 tends to be better determined than the distribution in period 2 because of the much better data constraints. Changes in the slip pattern can be seen more clearly by differencing the slip deficit distributions of two time periods. We adopt period 4 as the best estimate of the steady deformation (no SSEs in Lower Cook Inlet) and subtract its slip deficit rate distribution from that of the SSE periods (periods 1 and 3) to isolate the changes in the slip deficit distribution related to the SSEs (Figures 14 and 15). Here we focus mainly on the newly discovered SSE in Lower Cook Inlet as the Upper Cook Inlet events were studied recently [Fu and Freymueller, 2013; Fu et al., 2015]. As noted earlier, our division of the time series into four periods based on the velocity changes in Lower Cook Inlet is not ideal for the study of the Upper Cook Inlet SSEs, because the timing of events in the two regions is different.

Considering the model resolution limits, the areas of the SSEs in periods 1 and 3 may be the same; certainly, there is significant overlap between the two slip regions (Figure 14). Both are located underneath the southwestern Kenai Peninsula, with the updip and downdip limits being close to the Pacific and Cook Inlet shorelines, respectively. The earlier event may extend slightly farther to the northeast, while the later event may extend slightly farther to the southwest.

Averaged over an ~9 year long period, the earlier SSE (Figures 10 and 14) has a peak slip rate of ~110 mm/yr including the long-term relative average plate motion rate (55 mm/yr), and the slip rate averaged over its total slip area of 13,418 km<sup>2</sup> was 82 mm/yr. Over its ≥9 year duration, the cumulative geodetic moment of this SSE was  $4.97 \times 10^{20}$  N m ( $M_w \sim 7.8$ ), which is a minimum value as we cannot constrain the start time of the event. This SSE involves slip equivalent to 14 years of plate motion using the average slip rate. During the non-SSE time period (period 4: 2011.81–2014.87), the region of largest slip during the SSE has an average slip deficit rate of only ~20 mm/yr (range 10–30 mm/yr). If that is representative of the rate of slip deficit between SSEs, then the slip for a 9 year long SSE will be equivalent to ~38 years of steady deformation, which makes it possible that this event accounted for all of the accumulated slip deficit since the 1964 earthquake. On the other hand, the area between the two SSEs in Figure 14 (yellow coloring) is the result of a change from completely locked in period 1 to partially locked in period 4. This may be related to the trade-offs between SSEs and locking in the slip distribution, although even models that allow only positive slip deficit show some feature there (e.g., Figure 11b).

The SSE in period 3 has a peak slip rate of ~120 mm/yr and an average slip rate of 91 mm/yr over its 2 year duration. The geodetic moment of this SSE is  $6.98 \times 10^{19}$  N m ( $M_w \sim 7.2$ ). It thus accounts for about 4 years of plate motion or close to a decade of slip deficit accumulation. Although uncertainties remain

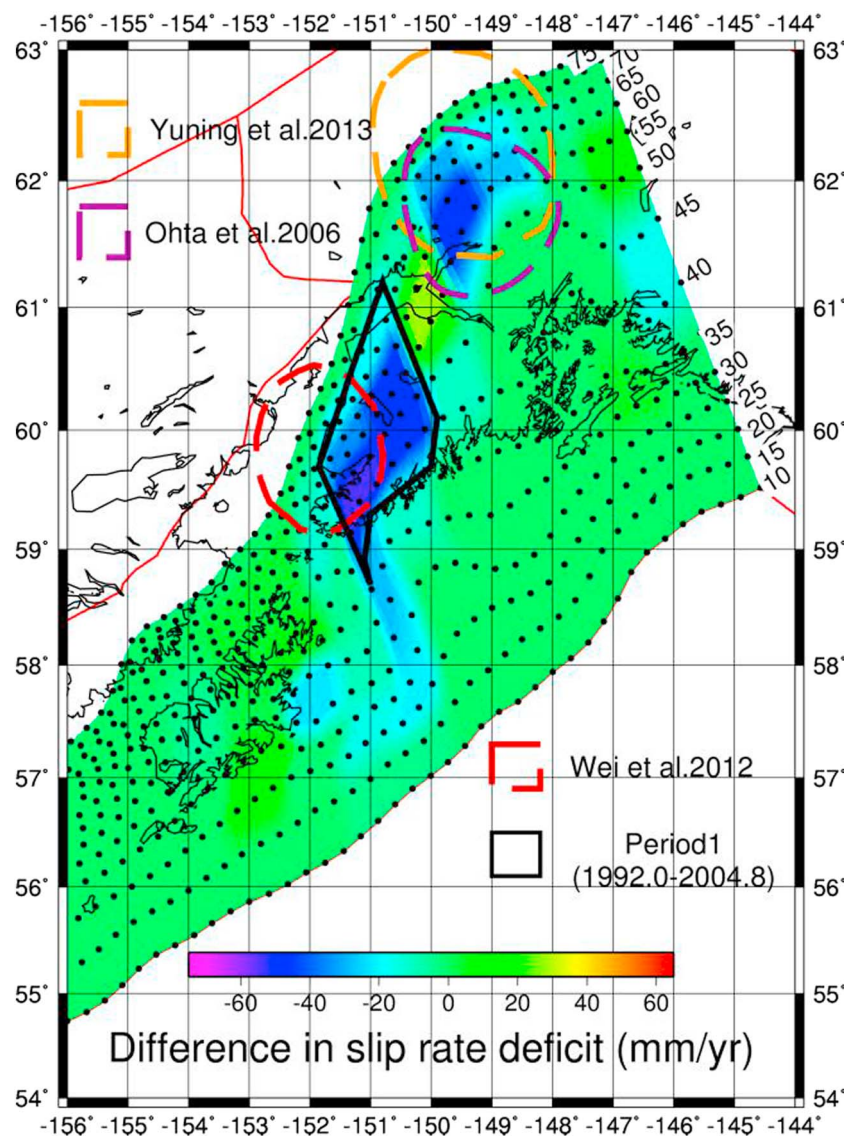


**Figure 14.** Inferred slip deficit rate distribution for the proposed 9 year long slow slip event (thick black polygon) in period 1 (1992.0–2004.8). The orange dashed circle shows the slow slip event proposed by *Fu and Freymueller [2013]*. The purple dashed circle shows the 1998–2001 slow slip event [*Ohta et al., 2006*]. The red dashed circle shows the slow slip event proposed by *Wei et al. [2012]*. The difference between the two model periods (period 1 and period 4 (2011.81–2014.87)) is shown using the same color scale as Figures 10–13.

large, the magnitude of slip in the period 3 SSE is similar to the total slip deficit in the region during period 2, and we propose that the duration of this second SSE was limited by the accumulated slip deficit after the first SSE.

Over most of the megathrust within the 1964 earthquake rupture area, the pattern of slip deficit remains the same for all four time periods, although model resolution is poor trenchward of the Pacific coast. In particular, the first-order pattern of along-strike variations in the downdip end of the main locked zone has not changed over the ~20 years of GPS data. However, the areas of slow slip immediately downdip of that show large changes in slip rates with time. The slip rates in the area of the lower Cook Inlet SSEs change abruptly from ~95 to 110 mm/yr in period 1 to ~25–55 mm/yr in period 2, which is smaller than the plate convergence rate (red box area in Figures 10 and 11). Then the slip rates change back to ~85–120 mm/yr in the next SSE (period 3) and finally change back to ~25–45 mm/yr in time period 4 (red box area in Figures 12 and 13). These slip rate changes are relatively abrupt. Also, the slip rates seem to be relatively constant during the slow slip

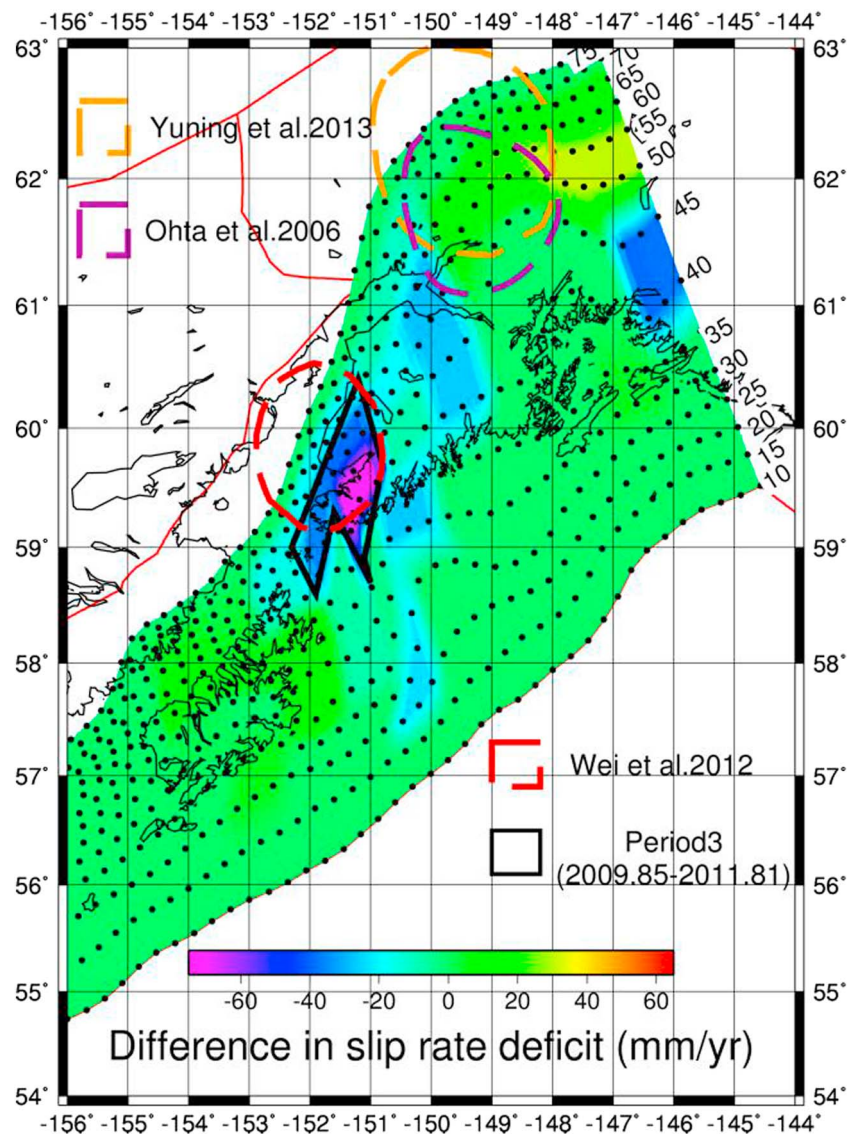


**Figure 15.** Inferred slip deficit rate distribution for the newly observed ~2 year long period slow slip event (thick black polygon) in period 3 (2009.85–2011.81). The orange, red, and purple dashed circles are as in Figure 14. The difference between the two model periods (period 3 and period 4 (2011.81–2014.87)) is shown using the same color scale as Figures 10–13.

events, as evidenced by nearly linear time series, rather than varying continually with time as in the Upper Cook Inlet SSEs. This suggests the possibility of some mechanical rate limit for slow slip in this area, although the mechanism that would lead to this is unclear. Note that the bounds on  $\phi$  in the inversion would have allowed slip at up to 3 times the rate of plate motion, so we do not think that this result is an artifact of the inversion. Updip of the SSEs we have identified here, there have been no observable significant changes of the locking fraction or slip deficit rates in the shallow zone. On parts of the model that have good resolution, the interface has remained completely locked over the last 20 years.

The red-orange areas in Figures 10–13 represent the completely locked area, and the yellow marks the transition from completely to partially locked which we refer to as the locking depth. There are clear along-strike variations in the depth of the transition in all four time periods. For time period (period 4), the locking depth is ~45 km in the Prince William Sound area, shallows to ~35 km under the Kenai Peninsula, and shallows again to ~25 km under the Kodiak Island (Figure 13). This is inversely correlated to the slab dip angle, in that the shallowest slab dip corresponds to the deepest locking depth, leading to a dramatic widening of the locked

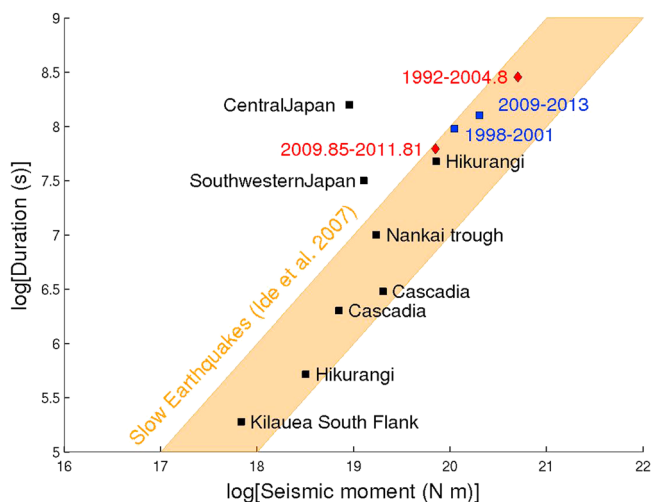


**Figure 16.** Moment versus duration of slow slip events in the Lower Cook Inlet in periods 1 and 3 compared to some at other subduction zones. The red diamonds show the Lower Cook Inlet SSEs (this study), and the blue squares show the Upper Cook Inlet SSEs, 1998–2001 [Ohta et al., 2006], and 2009–2013 [Fu and Freymueller, 2013]. Black squares show SSEs at other subduction zones [Ide et al., 2007; Kobayashi, 2014; Ochi and Kato, 2013; Wallace and Beavan, 2010]. The scaling relation for slow earthquakes as drawn by [Ide et al., 2007],  $M_o \propto T$ , is shown by an orange shaded area.

zone from southwest to northeast. The shallow-dipping slab corresponds to the subduction of the Yakutat block [Eberhart-Phillips et al., 2006].

## 5.2. Duration and Magnitude Scaling of the Lower Cook Inlet Slow Slip Events

Moment magnitudes for the two Lower Cook Inlet SSEs were computed in the previous section. We also calculate the moments of these SSEs based on differences of slip deficit rates between periods 1 and 4, between periods 3 and 4, and slip deficit rates inverted from differences of velocities between periods 1 and 4 and periods 3 and 4.

*Ide et al.* [2007] found a linear scaling between the log SSE duration ( $T$ ) and the log equivalent moment ( $M_o$ ) ( $M_o \propto T$ ) (Figure 16), which is different from that of normal earthquakes where  $M_o \propto T^3$ . From the two observed SSEs in the Lower Cook Inlet in this study and two previous observed SSEs in the Upper Cook Inlet, all four SSEs are located within the orange shaded area that marks the scaling relation  $M_o \propto T$  proposed by *Ide et al.* [2007]. All four Alaska events lie near the upper boundary of that area (Figure 16), and the best fit line based only on the Alaska SSEs has  $M_o \propto T^{1.3}$ . Compared with all global examples of SSEs, the newly observed 9 year long period SSE appears to be the longest SSE recorded geodetically so far. *Meade and Loveless* [2009] suggested that very long slow slip events would be difficult to distinguish from partial locking, because the slip rates would be comparable to or lower than plate motion rates. However, the 9 year SSE here has slip rates in excess of plate rates which make it observable geodetically but well within the slip rates suggested by *Meade and Loveless* [2009] for an event of this duration.

Evidence is increasing for the existence of decadal-scale or longer slow slip events or time variations in locking in multiple subduction zones. *Shennan and Hamilton* [2006] presented evidence for a possible slow event lasting 10–15 years that immediately preceded the 1964 Alaska earthquake. If the subsidence they inferred from changes in diatom assemblages resulted from a SSE, the slip would have occurred farther updip at shallower depth than any of the SSE observed geodetically [Fu and Freymueller, 2013; Ohta et al., 2006; Wei et al., 2012]. In the Sumatra subduction zone, coral paleogeodesy provides evidence for significant changes in uplift/subsidence rates over time [Meltzner et al., 2012; Meltzner et al., 2010]. Recent work has shown that an ~15 year long change in the uplift pattern in the Banyak Islands can be explained by the occurrence of a very long slow slip event [Meltzner et al., 2015; Tsang et al., 2015]. Scaling laws [*Ide et al.*, 2007; *Meade and Loveless*, 2009] do not suggest any clear upper limit for the duration or magnitude of slow slip events, and it is possible that as the time span of precise geodetic observations increases, longer and longer transient events may be found.

## 6. Conclusions

GPS time series for sites in Lower Cook Inlet, Alaska, show changes in velocity three times within the span 1995 to 2014: in late 2004, ~2010, and late 2011. The exact timing of the change in 2004 is weakly constrained because only two continuous GPS sites were operating at the time. However, the ~2010 and late 2011 velocity changes were abrupt, with the timing of the change determined within a few weeks at each site. Unlike the other slow slip events observed in Alaska, slip rates appear to be relatively constant during these slow slip events. The timing of each velocity change had a spatial progression, with the velocity changes propagating in either the updip or downdip direction.

We develop an improved block model for the region, which combines the Kenai Peninsula and Alaska Peninsula as a Peninsula block (PENN), along with Southern Alaska (SOAK) and Bering (BRNG) blocks. We estimate the angular velocity of the PENN block and a nominal average plate coupling variation simultaneously using a combination of periods 1 and 4, which have the best data constraints. We find that a single angular velocity fits data from all time periods well.

We then estimate the slip deficit rate distribution for the four time periods with two different limiting ranges of the locking fraction ( $\phi$ ):  $[-2, 1]$  and  $[0, 1]$ . The data require negative slip deficit rates in the Lower Cook Inlet area in periods 1 and 3, which indicates that slip rates were faster than plate convergence rates during these two time periods. The SSE in period 1 lasted at least 9 years, as it was already underway when our observations in that area begin in 1995. Another slow slip event in the same area lasted almost 2 years from the end of 2009 to the end of 2011.

The SSEs started and ended abruptly, within a period of a few months. The timing of velocity changes at individual sites suggests that at the start of these SSEs, the plate interface began to creep first at the downdip end, with the slip event propagating updip over a period of several weeks to a few months. Then, at the end of each event, the plate interface began to lock up first at the updip end, with the cessation of slip propagating downdip.

The 9 year long SSE in period 1 and the ~2 year long SSE in period 3 were both located at the same depth range of 40 to 60 km, at the downdip end of the locked zone. We find that the locking depth in the non-SSE time period is inversely correlated with the slab dip, with a deeper locking depth of ~45 km found in the Prince William Sound where the slab dip angle is shallowest. In the area of the Lower Cook Inlet slow events, between events the interface is fully locked to a depth of ~35 km and then partially locked to a depth of ~60 km.

## Acknowledgments

We appreciate Laura Wallace, David Schmidt, and another anonymous reviewer for providing helpful comments that significantly improve the manuscripts. We acknowledge EarthScope for the Plate Boundary Observatory (PBO) data and UNAVCO for operations of the PBO. All GPS data used in this work are archived at the UNAVCO or NGS/CORS archives. Tables in the supporting information contain site velocities for the four time periods and also the combined velocities of periods 1 and 4. This research was supported by NSF award EAR-1215933 to the University of Alaska Fairbanks. We use the Generic Mapping Tools (GMT) to draw the figures.

## References

- Altamimi, Z., X. Collilieux, and L. Métivier (2011), ITRF2008: An improved solution of the international terrestrial reference frame, *J. Geod.*, 85(8), 457–473.
- Argus, D. F., R. G. Gordon, M. B. Heflin, C. Ma, R. J. Eanes, P. Willis, W. R. Peltier, and S. E. Owen (2010), The angular velocities of the plates and the velocity of Earth's centre from space geodesy, *Geophys. J. Int.*, 180(3), 913–960.
- Brocher, T. M., G. S. Fuis, M. A. Fisher, G. Plafker, M. J. Moses, J. J. Taber, and N. I. Christensen (1994), Mapping the megathrust beneath the northern Gulf of Alaska using wide-angle seismic data, *J. Geophys. Res.*, 99(B6), 11,663–11,685, doi:10.1029/94JB00111.
- Cohen, S. C., and J. T. Freymueller (2004), Crustal deformation in the southcentral Alaska subduction zone, *Adv. Geophys.*, 47, 1–63.
- Cross, R. S., and J. T. Freymueller (2008), Evidence for and implications of a Bering plate based on geodetic measurements from the Aleutians and western Alaska, *J. Geophys. Res.*, 113, B07405, doi:10.1029/2007JB005136.
- DeMets, C., B. Márquez-Azúa, and E. Cabral-Cano (2014), A new GPS velocity field for the Pacific Plate—Part 1: Constraints on plate motion, intraplate deformation, and the viscosity of Pacific basin asthenosphere, *Geophys. J. Int.*, 199, 1878–1899.
- Dragert, H., K. Wang, and T. S. James (2001), A silent slip event on the deeper Cascadia subduction interface, *Science*, 292(5521), 1525–1528.
- Eberhart-Phillips, D., D. H. Christensen, T. M. Brocher, R. Hansen, N. A. Ruppert, P. J. Haussler, and G. A. Abers (2006), Imaging the transition from Aleutian subduction to Yakutat collision in central Alaska, with local earthquakes and active source data, *J. Geophys. Res.*, 111, B11303, doi:10.1029/2005JB004240.
- Elliott, J., J. T. Freymueller, and C. F. Larsen (2013), Active tectonics of the St. Elias orogen, Alaska, observed with GPS measurements, *J. Geophys. Res. Solid Earth*, 118, 5625–5642, doi:10.1002/jgrb.50341.
- Fletcher, H. J. (2002), *Crustal Deformation in Alaska Measured Using the Global Positioning System*, Univ. of Alaska, Fairbanks.
- Freed, A. M., R. Bürgmann, E. Calais, J. Freymueller, and S. Hreinsdóttir (2006), Implications of deformation following the 2002 Denali, Alaska, earthquake for postseismic relaxation processes and lithospheric rheology, *J. Geophys. Res.*, 111, B01401, doi:10.1029/2005JB003894.
- Freymueller, J. T., H. Woodard, S. C. Cohen, R. Cross, J. Elliott, C. F. Larsen, S. Hreinsdóttir, and C. Zweck (2008), Active deformation processes in Alaska, based on 15 years of GPS measurements, *Act. Tecton. Seism. Potential Alaska*, 179, 1–42.
- Fu, Y., and J. T. Freymueller (2013), Repeated large slow slip events at the southcentral Alaska subduction zone, *Earth Planet. Sci. Lett.*, 375, 303–311.
- Fu, Y., J. T. Freymueller, and T. Jensen (2012), Seasonal hydrological loading in southern Alaska observed by GPS and GRACE, *Geophys. Res. Lett.*, 39, L15310, doi:10.1029/2012GL052453.
- Fu, Y., Z. Liu, and J. T. Freymueller (2015), Spatiotemporal variations of the slow slip event between 2008 and 2013 in the southcentral Alaska subduction zone, *Geochem. Geophys. Geosyst.*, 16, 2450–2461, doi:10.1002/2015GC005904.

- Furumoto, A. S. (1965), Analysis of Rayleigh wave: Part II, in *Source Mechanism Study of the Alaska Earthquake and Tsunami of March 27, 1964, Rep. HIG-65-17*, pp. 31–42, Univ. of Hawaii, Institute of Geophysics, Honolulu.
- Hayes, G. P., D. J. Wald, and R. L. Johnson (2012), Slab1.0: A three-dimensional model of global subduction zone geometries, *J. Geophys. Res.*, 117, B01302, doi:10.1029/2011JB008524.
- Ide, S., G. C. Beroza, D. R. Shelly, and T. Uchide (2007), A scaling law for slow earthquakes, *Nature*, 447(7140), 76–79.
- Johnson, K. M., R. Bürgmann, and J. T. Freymueller (2009), Coupled afterslip and viscoelastic flow following the 2002 Denali Fault, Alaska earthquake, *Geophys. J. Int.*, 176(3), 670–682.
- Kobayashi, A. (2014), A long-term slow slip event from 1996 to 1997 in the Kii Channel, Japan, *Earth Planets Space*, 66(1), 1–7.
- Kostoglodov, V., S. K. Singh, J. A. Santiago, S. I. Franco, K. M. Larson, A. R. Lowry, and R. Bilham (2003), A large silent earthquake in the Guerrero seismic gap, Mexico, *Geophys. Res. Lett.*, 30(15), 1807, doi:10.1029/2003GL017219.
- Lahr, J. C., and G. Plafker (1980), Holocene Pacific–North American plate interaction in southern Alaska: Implications for the Yakataga seismic gap, *Geology*, 8(10), 483–486.
- McCaffrey, R. (2002), Crustal block rotations and plate coupling, *Plate Boundary Zones*, 101–122.
- McCaffrey, R. (2009), Time-dependent inversion of three-component continuous GPS for steady and transient sources in northern Cascadia, *Geophys. Res. Lett.*, 36, L07304, doi:10.1029/2008GL036784.
- Meade, B. J., and J. P. Loveless (2009), Predicting the geodetic signature of  $M_W \geq 8$  slow slip events, *Geophys. Res. Lett.*, 36, L01306, doi:10.1029/2008GL036364.
- Meltzner, A. J., K. Sieh, H. W. Chiang, C. C. Shen, B. W. Suwargadi, D. H. Natawidjaja, B. E. Philibosian, R. W. Briggs, and J. Galetzka (2010), Coral evidence for earthquake recurrence and an AD 1390–1455 cluster at the south end of the 2004 Aceh–Andaman rupture, *J. Geophys. Res.*, 115, B10402, doi:10.1029/2010JB007499.
- Meltzner, A. J., K. Sieh, H. W. Chiang, C. C. Shen, B. W. Suwargadi, D. H. Natawidjaja, B. Philibosian, and R. W. Briggs (2012), Persistent termini of 2004- and 2005-like ruptures of the Sunda megathrust, *J. Geophys. Res.*, 117, B04405, doi:10.1029/2011JB008888.
- Meltzner, A. J., K. Sieh, H.-W. Chiang, C.-C. Wu, L. L. Tsang, C.-C. Shen, E. M. Hill, B. W. Suwargadi, D. H. Natawidjaja, and B. Philibosian (2015), Time-varying interseismic strain rates and similar seismic ruptures on the Nias–Simeulue patch of the Sunda megathrust, *Quat. Sci. Rev.*, 122, 258–281.
- Nishimura, T., T. Matsuzawa, and K. Obara (2013), Detection of short-term slow slip events along the Nankai Trough, southwest Japan, using GNSS data, *J. Geophys. Res. Solid Earth*, 118, 3112–3125, doi:10.1002/jgrb.50222.
- Ochi, T., and T. Kato (2013), Depth extent of the long-term slow slip event in the Tokai district, central Japan: A new insight, *J. Geophys. Res. Solid Earth*, 118, 4847–4860, doi:10.1002/jgrb.50355.
- Ohta, Y., J. T. Freymueller, S. Hreinsdóttir, and H. Suito (2006), A large slow slip event and the depth of the seismogenic zone in the south central Alaska subduction zone, *Earth Planet. Sci. Lett.*, 247(1), 108–116.
- Okada, Y. (1985), Surface deformation due to shear and tensile faults in a half-space, *Bull. Seismol. Soc. Am.*, 75(4), 1135–1154.
- Peng, Z., and J. Gomberg (2010), An integrated perspective of the continuum between earthquakes and slow-slip phenomena, *Nat. Geosci.*, 3(9), 599–607.
- Press, W. H. (1989), *Numerical Recipes in Pascal: The Art of Scientific Computing*, Cambridge Univ. Press, New York.
- Savage, J. (1983), A dislocation model of strain accumulation and release at a subduction zone, *J. Geophys. Res.*, 88(6), 4984–4996, doi:10.1029/JB088iB06p04984.
- Schwartz, S. Y., and J. M. Rokosky (2007), Slow slip events and seismic tremor at circum-Pacific subduction zones, *Rev. Geophys.*, 45, RG3004, doi:10.1029/2006RG000208.
- Sella, G. F., S. Stein, T. H. Dixon, M. Craymer, T. S. James, S. Mazzotti, and R. K. Dokka (2007), Observation of glacial isostatic adjustment in “stable” North America with GPS, *Geophys. Res. Lett.*, 34, L02306, doi:10.1029/2006GL027081.
- Shennan, I., and S. Hamilton (2006), Coseismic and pre-seismic subsidence associated with great earthquakes in Alaska, *Quat. Sci. Rev.*, 25(1), 1–8.
- Suito, H., and J. T. Freymueller (2009), A viscoelastic and afterslip postseismic deformation model for the 1964 Alaska earthquake, *J. Geophys. Res.*, 114, B11404, doi:10.1029/2008JB005954.
- Szeliga, W., T. I. Melbourne, M. M. Miller, and V. M. Santillan (2004), Southern Cascadia episodic slow earthquakes, *Geophys. Res. Lett.*, 31, L16602, doi:10.1029/2004GL020824.
- Tsang, L. L., A. J. Meltzner, B. Philibosian, E. M. Hill, J. T. Freymueller, and K. Sieh (2015), A 15-year slow slip event on the Sunda megathrust offshore Sumatra, *Geophys. Res. Lett.*, 42, 6630–6638, doi:10.1002/2015GL064928.
- Wallace, L. M., and J. Beavan (2010), Diverse slow slip behavior at the Hikurangi subduction margin, New Zealand, *J. Geophys. Res.*, 115, B12402, doi:10.1029/2010JB00771.
- Wei, M., J. J. McGuire, and E. Richardson (2012), A slow slip event in the south central Alaska subduction zone and related seismicity anomaly, *Geophys. Res. Lett.*, 39, L15309, doi:10.1029/2012GL052351.